Nanoscale

ROYAL SOCIETY OF CHEMISTRY

PAPER

View Article Online
View Journal | View Issue



Cite this: *Nanoscale*, 2025, **17**, 4543

# Enhanced detection of Brain-Derived Neurotrophic Factor (BDNF) using a reduced graphene oxide field-effect transistor aptasensor†

Mostafa Salehirozveh, [a] Robin Bonné,[b] Peeyush Kumar,[c] Farbod Abazar, [d] Parisa Dehghani,*[e] Ivan Mijakovic*[a,g] and Vellaisamy A. L. Roy[e,f]

Neurodegenerative diseases, characterized by the progressive deterioration of neuronal function and structure, pose significant global public health and economic challenges. Brain-Derived Neurotrophic Factor (BDNF), a key regulator of neuroplasticity and neuronal survival, has emerged as a critical biomarker for various neurodegenerative and psychiatric disorders, including Alzheimer's disease. Traditional diagnostic methods, such as Enzyme-Linked Immunosorbent Assay (ELISA) and electrochemiluminescence (ECL) assays, face limitations in terms of sensitivity, stability, reproducibility, and cost-effectiveness. In this research, we developed the first electrical aptasensor for BDNF detection, constructed on a flexible polyimide (PI) membrane coated with reduced graphene oxide (r-GO) and utilized an extended-gate field-effect transistor (EGFET) as the transducer. Comprehensive characterization of the sensor, coupled with the fine-tuning of aptamer concentration and the binding time of DNA aptamers to the chemical linker, was achieved through Electrochemical Impedance Spectroscopy (EIS) to boost sensitivity. Consequently, by utilizing the unique properties of r-GO and DNA aptamers, the aptasensor exhibited exceptional detection abilities, with a detection limit as low as 0.4 nM and an extensive response range spanning from 0.025 to 1000 nM. The flexible PI-based electrode offers exceptional stability, affordability, and durability for home diagnostics, enriched by the reusability of its electronic transducer, making the device highly portable and suitable for prolonged monitoring. Our aptasensor surpasses traditional methods, showcasing superior real-time performance and reliability. The high sensitivity and specificity of our aptasensor highlight its potential to significantly improve early diagnosis and therapeutic monitoring of neurodegenerative diseases such as Alzheimer's, representing a considerable advancement in the diagnosis and management of such conditions.

Received 12th October 2024,
Accepted 23rd December 2024

DOI: 10.1039/d4nr04228j

rsc.li/nanoscale



## Introduction

Neurodegenerative diseases are marked by the progressive deterioration of neuronal function and structure, often culminating in the disorder and death of neuronal cells.[1] Millions of individuals are afflicted by these conditions, which manifest through clinical symptoms including disrupted selective functions, neuroinflammation, neuronal and synaptic damage, and protein aggregation. The impact of neurodegenerative diseases on public health and the economy is profound. However, the incomplete understanding of these diseases in all their facets has hindered the development of effective clinical treatments.[2,3] Neurodegenerative disorders have reached pandemic proportions globally, with most remaining incurable due to the unclear mechanisms underlying these diseases and the lack of effective clinical therapies. The limited number of clinical treatments available have largely failed in therapeutic application, primarily because there are no commercially available methods for early diagnosis based on specific biomarkers at initial stages of the neurodegenerative diseases.[2,4]

Brain-derived neurotrophic factor (BDNF) is a regulatory protein essential for modulating neuroplasticity and neuronal survival in the nervous system, playing a critical role in

[a]*Division of Systems and Synthetic Biology, Department of Life Sciences, Chalmers University of Technology, SE-41296 Gothenburg, Sweden*
[b]*Center for Electromicrobiology (CEM), Aarhus University, Ny Munkegade 114, 8000 Aarhus, Denmark*
[c]*Department of Engineering, Johannes Kepler University Linz – JKU, Austria*
[d]*Department of Information Engineering, University of Pisa, UNIPI, Pisa, Italy*
[e]*James Watt School of Engineering, University of Glasgow, Glasgow G12 8QQ, UK. E-mail: Parisa.Dehghani@glasgow.ac.uk*
[f]*School of Science and Technology, Hong Kong Metropolitan University, Ho Man Tin, Hong Kong*
[g]*The Novo Nordisk Foundation Center for Biosustainability, Technical University of Denmark, DK-2800 Kongens Lyngby, Denmark. E-mail: ivan.mijakovic@chalmers.se, ivmi@biosustain.dtu.dk*

† Electronic supplementary information (ESI) available. See DOI: https://doi.org/10.1039/d4nr04228j

memory and learning. It is critically involved in promoting neurons' growth, repair, differentiation, and survival.[5] BDNF is a significant biomarker for a range of neurological and psychiatric disorders. Its levels in blood serum can vary substantially depending on factors such as age, gender, and overall health. Diminished BDNF levels are correlated with neurodegenerative diseases, including Alzheimer's disease, Parkinson's disease, Huntington's disease, and multiple sclerosis.[6–9] While some studies provide vague evidence regarding the use of BDNF as a biomarker for neurodegenerative diseases,[10,11] numerous meta-analyses confirm the correlation between brain disorders and serum BDNF.[12,13]

Enzyme-linked immunosorbent assay (ELISA) is considered the gold standard technique and can routinely be used for BDNF diagnosis in clinical trials. Nevertheless, the accuracy of the measurements is called into question due to variations observed among different commercially available ELISA kits used on the same human serum samples.[14] On the other hand, the low sensitivity, stability, and high cost of current biosensors and sensing platforms for BDNF detection underscore the urgent demand for the development of novel analytical tools based on sensitive recognition elements with high specificity.[15] These tools should enable the rapid detection of BDNF to improve the early diagnosis of neurodegenerative diseases and expedite therapeutic interventions. To address the limitations of the most used analytical technologies, the development of flexible graphene-based biosensors has gained significant attention. These biosensors offer unique characteristics, such as high sensitivity, excellent mechanical, optical, and electrical properties, and broad applications in the field of biosensing. In this context, traditional diagnostic strategies based on antibody–antigen interactions encounter issues such as reduced stability and limited shelf life. Conversely, the aptamer-based approach offers several advantages. Aptamers, with their streamlined and cost-effective production processes, ensure reduced batch-to-batch variation and eliminate the need for an immune response or the use of animals in their production. These characteristics expedite manufacturing and enhance the stability and longevity of biosensors, making aptamers an ideal candidate for biosensor applications.[16,17]

Graphene-based nanomaterials demonstrate ambipolar transfer characteristics and exceptionally high electrical conductivity (200 000 $cm^2 V^{-1} s^{-1}$), rendering them highly suitable for a broad spectrum of applications. These encompass nanoenergy,[18] batteries,[19,20] energy storage, surface engineering,[21] and biosensing.[22–24] Graphene oxide (GO) is recognised as a highly promising material with significant potential for use in various ultra-sensitive biosensors, particularly graphene-based field-effect transistor (G-FET) biosensors. The exceptional sensitivity of graphene oxide FET biosensors is attributed to the adsorption of molecules, which induces charge transfer on the extended gate surface. This process alters the conductivity of graphene oxide and results in a shift in the Fermi energy.[25] Additionally, the conductivity of graphene oxide can be modified by molecule adsorption on its surface, even without shifts in the Fermi energy. Accordingly, the non-covalent binding of target biomolecules to graphene oxide can significantly modify the carrier density and electrical conductivity of graphene-based FETs, even at low biomolecule concentrations.

Metal–oxide–semiconductor field-effect transistors (MOSFETs), functioning as transducers, generate electronic signals with high sensitivity in response to specific biochemical reactions, making them widely utilized in the development of biosensors. The extended gate FET (EG-FET) variant effectively addresses application drawbacks by extending the recognition sites.[26–29] The configuration of EGFETs makes them highly suitable for biosensing applications due to the adjustable and replaceable recognition sites on the sensing platform, tailored to specific targets. To the best of our knowledge, there are no reports on the design and fabrication of graphene oxide EGFETs for BDNF detection. In this study, a comprehensive characterization of the sensor, in conjunction with the meticulous optimization of aptamer concentration and the binding duration of DNA aptamers to the chemical linker, was accomplished through Electrochemical Impedance Spectroscopy (EIS) to enhance sensitivity. This research pioneers the use of DNA aptamers for BDNF detection *via* EIS and reduced graphene oxide field-effect transistors (r-GOFETs), representing a significant advancement in biosensing technology.[7,8] As a result, by leveraging the distinctive properties of reduced graphene oxide (r-GO) and DNA aptamers, the aptasensor demonstrated remarkable detection capabilities, achieving a detection threshold as low as 0.4 nM and maintaining an extensive linear response range extending from 0.025 to 1000 nM. The adaptable polyimide (PI)-based electrode provides outstanding stability, cost-effectiveness, and longevity for at-home diagnostics, further augmented by the reusability of its electronic transducer, rendering the device highly portable and appropriate for extended monitoring. This advancement provides a powerful tool for early neurodegenerative disease diagnosis. In addition, we have developed gold (Au) and silver chloride (Ag/AgCl) electrodes on flexible polymer (polyimide) substrates, which offer high stability and make long-term monitoring possible.[7] These flexible electrodes are compared with conventional methods, demonstrating superior performance and reliability. Flexible biosensors are at the forefront of a rapidly expanding research field, utilizing multidisciplinary approaches in materials science, fabrication techniques, and design innovations.

## Results and discussion

### Pseudo-reference electrode characterization

An alternative approach for depositing the silver layer involves using undiluted aqueous $FeCl_3$ solutions for chemical oxidation. The primary objective of the proposed pseudo-reference electrode fabrication method is to develop a fully compatible large-scale production process. In this study, a homogeneous AgCl-coated layer is depicted in Fig. S1a.† Energy-dispersive X-ray (EDX) analysis further confirms the formation of the AgCl layer, evidenced by the presence of a chlorine peak in

 

addition to the silver peak (Fig. S1b and c†). The performance of the electrode was evaluated through electrochemical characterization using cyclic voltammetry (CV) in a buffer solution. The initial assessment involved varying the scan rate and comparing the results with those obtained by using a commercial Ag/AgCl electrode.

As shown in Fig. S1d,† there is no significant difference between the CV curves of the fabricated pseudo-reference electrode and the commercial Ag/AgCl electrode, indicating comparable performance and validating the efficacy of the fabrication method.[30]

### Characterization of the aptasensor

A schematic representation of the aptasensor's structure is presented in Fig. 1a. Each step involved in electrode modification was characterized using Electrochemical Impedance Spectroscopy (EIS). The Nyquist plots, depicting the impedance spectra of various electrode configurations after each step of modification, are shown in Fig. 1b. Here, the results demonstrate that modification of the bare glassy carbon (GC) electrode (plot a) with a GO film (plot b) leads to a significant increase in $R_{ct}$. Specifically, the introduction of GO onto the GC electrode surface results in a marked elevation in the $R_{ct}$ value compared to the unmodified GC electrode, due to the interaction between the electrolyte species in the solution and the oxygen-containing functional groups on the GO sheet-based electrode.[31–34] However, this trend is somewhat reversed when considering the GC/r-GO electrode. After the reduction of GO by hydrazine, the $R_{ct}$ decreases (plot d). This decline in $R_{ct}$ can be attributed to the high conductivity and substantial surface area of r-GO, which promotes and facilitates the charge transfer process at the electrode interface.[35–37] When the graphene sensor surfaces were modified with 1-pyrenebutanoic acid succinimidyl ester (GC/r-GO/PBASE), a molecular linker, the $R_{ct}$ exhibited only a slight shift, and the electron transfer resistance showed a modest increase (plot e).[38,39] Subsequently, after incubation with aptamer molecules (GC/r-GO/PBASE/APT), the $R_{ct}$ values increase significantly (plot e). This heightened signal can be attributed to two factors: the blocking effect of the aptamer molecules on the electrode surface and the repulsive force between the negatively charged phosphate groups of DNA and the redox probe.[40] Additionally, the adsorption of BSA onto the surface of the GC/r-GO/PBASE/APT electrode results in a further increase in the $R_{ct}$ value (plot

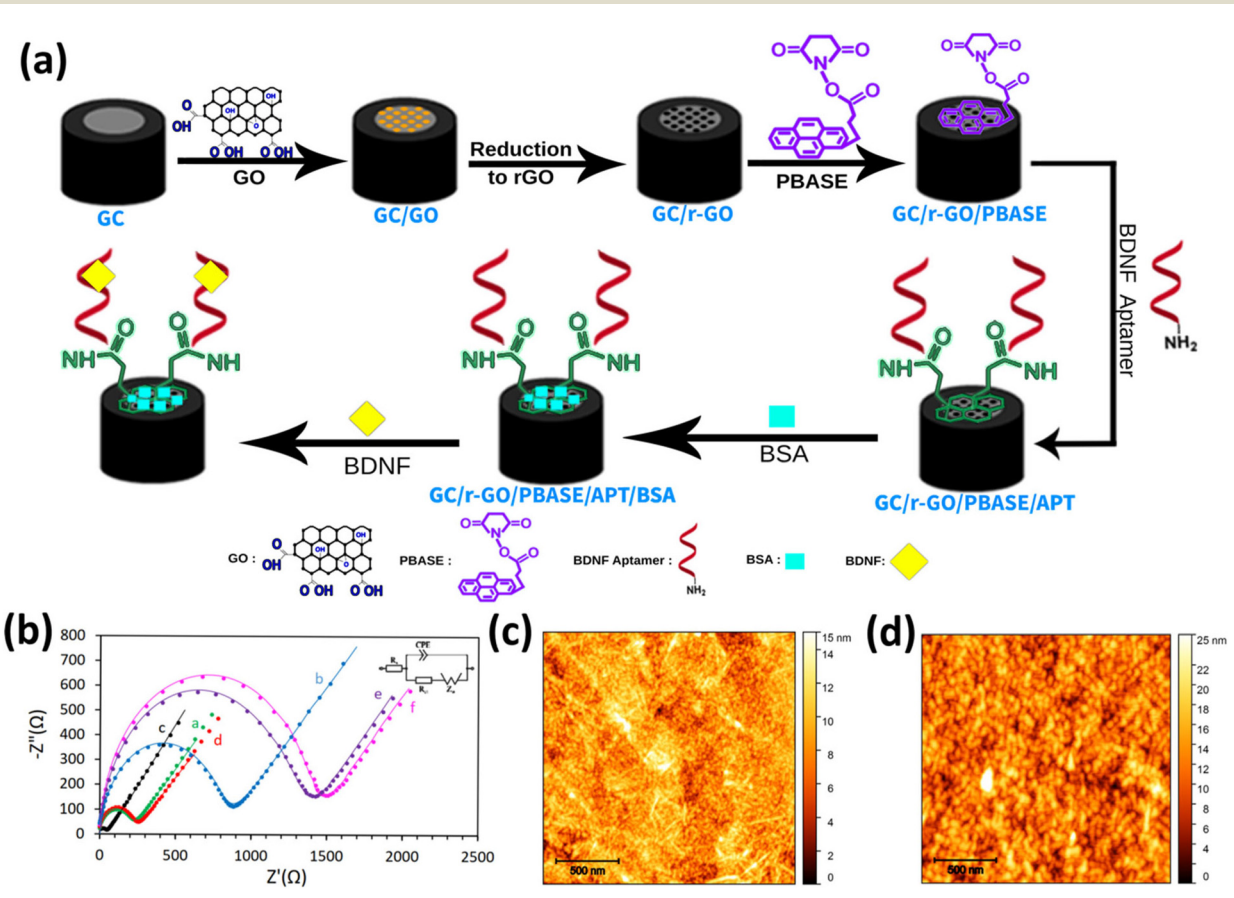


**Fig. 1** (a) Schematic diagram of the fabrication and operation of the aptasensor. (b) EIS complex plane plots obtained on (a) GC, (b) GC/GO, (c) GC/rGO, (d) GC/rGO/PBASE, (e) GC/rGO/PBASE/APT and (f) GC/rGO/PBASE/APT/BSA electrodes in 0.1 M KCl electrolyte solution containing 10 mM $K_3[Fe(CN)_6]/K_4[Fe(CN)_6]$. Here, dotted and dashed lines represent the experimental and fitted data, respectively, based on the modified Randles model (inset of the figure). AFM images of the GC/rGO/PBASE/APT electrode (c) after binding with BDNF (d).

f). These results are consistent with findings from recent studies, confirming the reliability and validity of our observations. Consequently, the presence of BDNF leads to a substantial increase in the $R_{ct}$ value. The Randles model parameters are presented in Table S1.†

To gain deeper insights into the immobilization of aptamer molecules on the electrode surface, Atomic Force Microscopy (AFM) analysis was performed on GC/r-GO/PBASE and GC/r-GO/PBASE/APT-modified electrodes. The root mean square (RMS) surface roughness values were determined to be approximately 2 nm and 4 nm, respectively, as shown in Fig. 1c and d. These findings confirm the successful binding between BDNF and DNA aptamers, as evidenced by the increased surface roughness.

These results are consistent with prior literature findings,[23,41,42] and affirm the high density of BDNF-aptamer and BDNF binding affinity to the electrode surface, in excellent agreement with the EIS results. Also, the elemental structure of the synthesized GO was characterized by FTIR and XRD (Fig. S2†). Here, in the FTIR image of GO, the vibration peaks observed include ~1058 $cm^{-1}$ (C–O–C), ~1228 $cm^{-1}$ (C–O), and ~1622 $cm^{-1}$ (C═C). Additionally, there are bending vibration peaks at ~1374 $cm^{-1}$ (O–H) and stretching vibrations at ~1740 $cm^{-1}$ (C═O). A broad peak in the range of 3200–3500 $cm^{-1}$ is attributed to O–H stretching from alcohol groups and water molecules, superimposed on the O–H bending vibrations of COOH groups. Moreover, the structural properties of the synthesized GO were studied by XRD analysis, illustrating the distinct XRD peak of GO at ~10°. These results confirm the success of the oxidation process during GO synthesis and indicate the presence of numerous oxygen-containing functional groups on the GO surface.

### Optimization of analytical parameters

To achieve the highest sensitivity of the proposed aptasensor, several key experimental parameters, such as aptamer incubation time and aptamer concentration, were thoroughly investigated and optimized using the EIS technique. The experimental results reveal that a 1-hour incubation period was sufficient for DNA aptamers to interact effectively with PBASE, leading to the maximum $\Delta R_{ct}$ (Fig. 2a). Various aptasensors were developed using different aptamer concentrations, and 12.5 nM BDNF was employed to compare the response of the aptasensors in terms of their $\Delta R_{ct}$. The concentration of the aptamers significantly influences the detection capability of the aptasensor, as illustrated in Fig. 2b. Fig. 2c and d show that as the aptamer concentration increases from 2 to 10 μM, the $R_{ct}$ intensity gradually enhances. The maximum $\Delta R_{ct}$ for 12.5 nM BDNF protein was achieved at an aptamer concentration of 6.0 μM. Beyond this concentration, $\Delta R_{ct}$ slightly decreases. This decrease may be attributed to an excess of aptamers on the electrode surface, which can hinder the

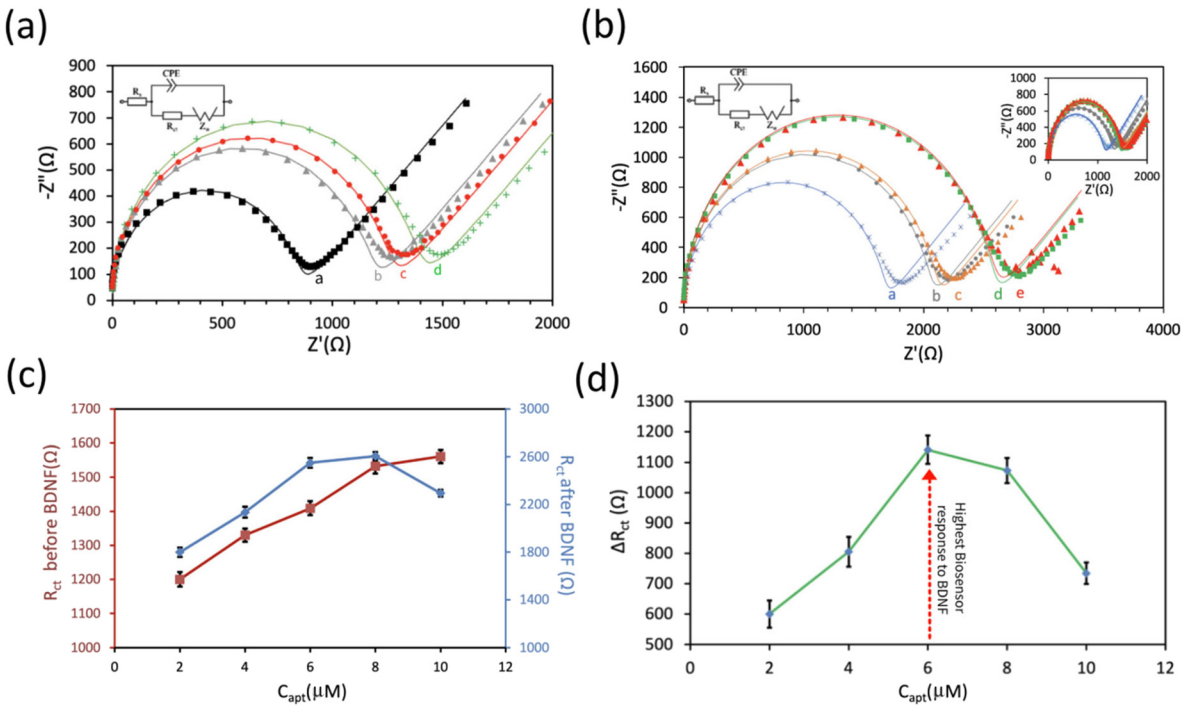


**Fig. 2** (a) EIS complex plane plots were obtained for GC/r-GO/PBASE/APT at different aptamer incubation times in 0.1 M KCl electrolyte solution containing 10 mM $K_3[Fe(CN)_6]/K_4[Fe(CN)_6]$. (b) EIS complex plane plots obtained for GC/r-GO/PBASE/APT at different aptamer concentrations and its response to 12.5 nM BDNF in 0.1 M KCl electrolyte solution containing 10 mM $K_3[Fe(CN)_6]/K_4[Fe(CN)_6]$. Here, dotted and dashed lines represent the experimental and fitted data, respectively, based on the modified Randles model (inset of the figure). (c) Extracted $R_{ct}$ from the plot (b). (d) The $\Delta R_{ct}$ of the GC/r-GO/PBASE/APT electrode with different aptamer concentrations (2 to 10 μM) and 12.5 nM BDNF protein.

necessary conformational change when the aptamer binds to the BDNF protein, making the redox moiety less accessible to the electrode surface.[43–45] Consequently, an incubation time of 1 hour and an aptamer concentration of 6 μM were determined to be the optimal conditions for aptamer binding to the surface of the GC/r-GO/PBASE electrode.

### Analytical performance of the aptasensor

To evaluate the analytical performance of the proposed aptasensor, a range of BDNF concentrations from 0.025 to 1000 nM was employed, and the corresponding Nyquist plots and aptasensor responses were recorded (as illustrated in Fig. 3a). As the BDNF concentration increased, a noticeable change in the Nyquist plots was observed, characterized by a significant increase in the $R_{ct}$ value. The obtained data are illustrated in Fig. 3b, which demonstrates the aptasensor response as a function of the BDNF concentration. A linear increase in the aptasensor response is evident as the BDNF concentration rises, as described by using eqn (1).

$$\Delta R_{ct}\ (\Omega) = 95.51[\text{BDNF}]\ (\text{nM}) + 41.63 \quad R^2 = 0.97 \qquad (1)$$

At high BDNF concentrations, the calibration curve deviates from linearity due to the saturation of the electrode surface.

From eqn (1), the estimated limit of detection (LOD) and sensitivity for the GC/r-GO/PBASE/APT/BSA electrode were determined as 31.3 nM (S/N = 3) and 95.5 Ω $nM^{-1}$, respectively. The selectivity of the proposed aptasensor was investigated in the presence of some interfering species such as glial cell line-derived neurotrophic factor (GDNF), nerve growth factor (NGF), Prostate-Specific Antigen (PSA), and human epidermal growth factor receptor 2 (HER2). These proteins were chosen because of their structural resemblance to BDNF.[46] As illustrated in Fig. 3c, a significant response is noted only with the addition of BDNF, while the response to 10 μM of any other species is less than 1% of the response elicited by 50 nM BDNF. These results demonstrate the high accuracy and selectivity of the proposed aptasensor in the complex matrix of human blood serum. The high selectivity of the aptasensor was attributed to the effective immobilization of BDNF aptamer molecules and the efficient blocking effect of BSA on the GC/r-GO/PBASE/APT/BSA electrode. To confirm that the observed signal originated from the specific interaction between the aptamer and BDNF, a synthesized mutated non-binding aptamer was immobilized on the sensor surface. As anticipated, no significant response was observed upon exposure to BDNF or other biomolecules, as shown in Fig. S3a.† Furthermore, the long-term stability and performance of the sensors were evaluated over a 30-day period using three independent sensors. The relative response exhibited a decline of approximately 7% after 5 days and 21% after 30 days, as illustrated in Fig. S3b,† indicating acceptable stability over the investigated timeframe.

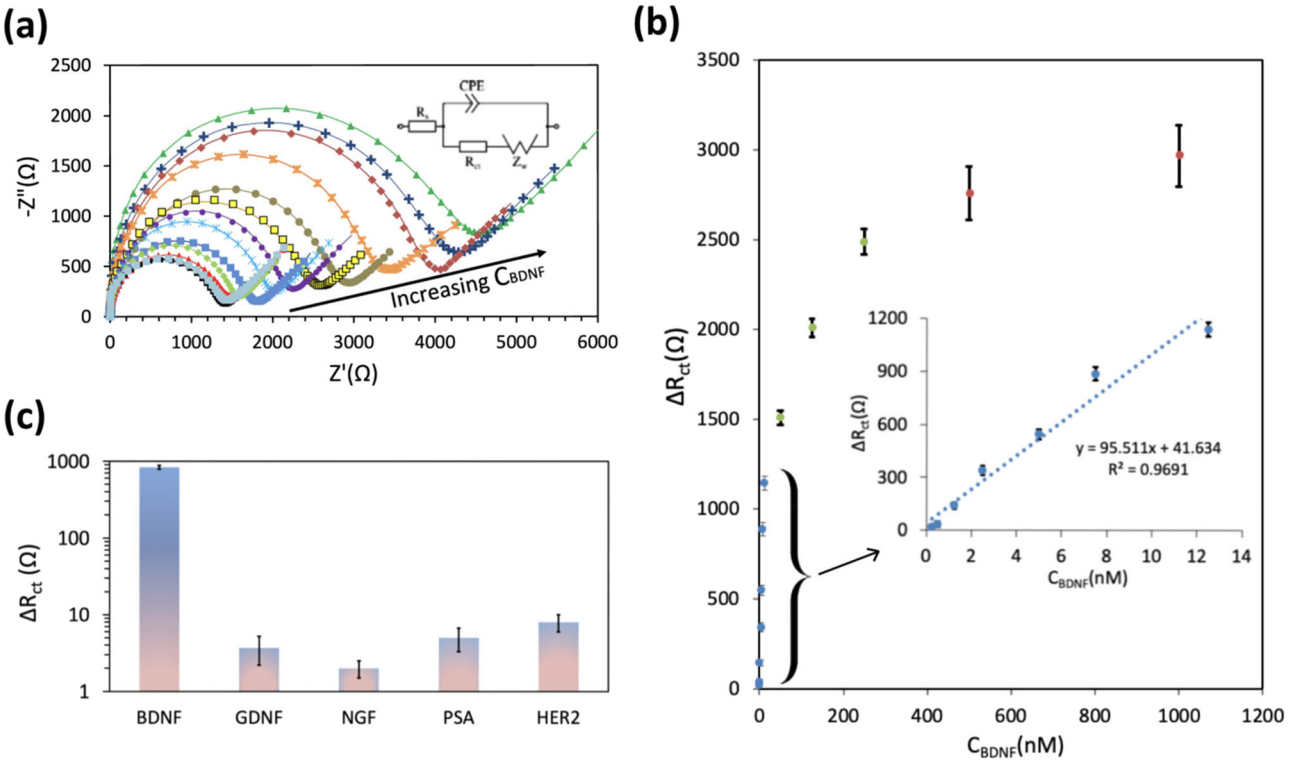


**Fig. 3** (a) Nyquist plots of the aptasensor at various concentrations of BDNF. Here, dotted and dashed lines represent the experimental and fitted data, respectively, based on the modified Randles model (inset of the figure). (b) Calibration curve of the aptasensor in the probe solution with different BDNF concentrations from 0.025 to 1000 nM. The inset displays the resulting linear range. (c) Selectivity of the aptasensor for BDNF detection compared to other biological interferents. BDNF was used at 50 nM, while the other tested molecules were each used at 10 μM.

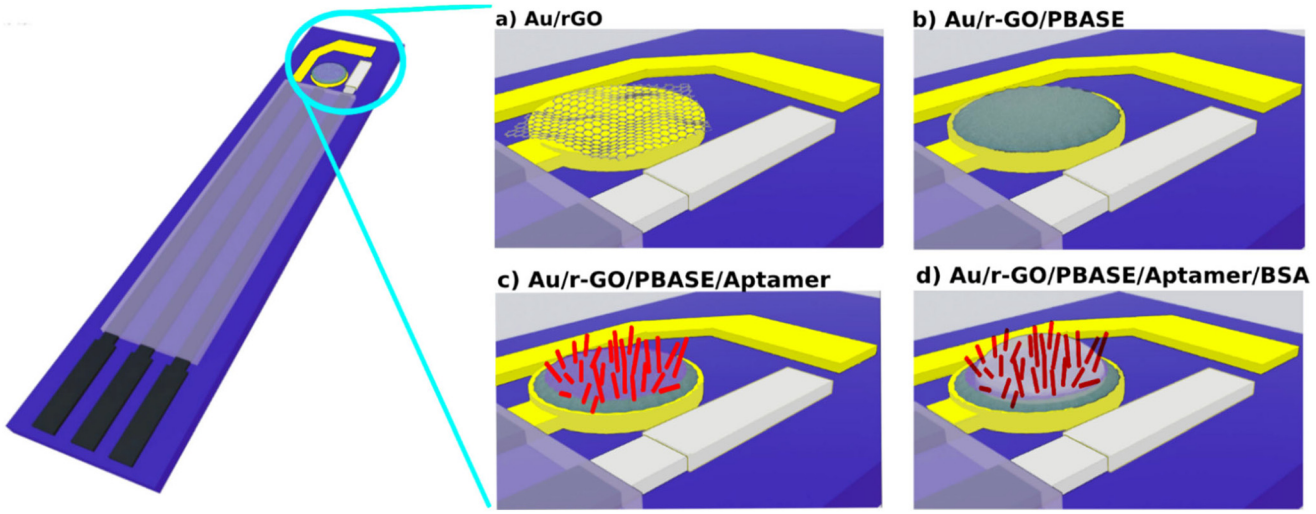


**Fig. 4** (a) Schematic image of the Au electrode deposited on the surface of polyimide (PI). The functionalization of the modified r-GO/PBASE electrode (b) before and (c) after aptamer immobilization and (d) after blocking the surface with BSA is illustrated. Here, the aptamers are presented by red rods.

### BDNF detection with EGFET

As illustrated in the schematic in Fig. 4, the flexible polyimide (PI) electrode serves as an extended sensing element and was modified with r-GO/PBASE/APT/BSA within an extended-gate field-effect transistor configuration (aptaEGFET). This design capitalizes on the selective properties of the r-GO/PBASE/APT/BSA electrode, which was specifically engineered to recognize and bind to BDNF. When incorporated into the EGFET system, the binding of BDNF induces changes in the electrical properties of the r-GO/PBASE/APT/BSA electrode, which are then transduced into measurable signals. This configuration is optimized to provide high sensitivity and selectivity for BDNF, making it an effective tool for detecting and quantifying BDNF in complex sample matrices. In this EGFET setup, the gate terminal of the conventional n-MOSFET functions as the transducer, interfacing with the molecular recognition component of the sensor.

The negatively charged aptamers, which serve as recognition sites on the surface of the modified electrode, enable the specific binding of BDNF within the r-GO/PBASE/APT/BSA modified electrode matrix. Applying a positive bias to the floating gate electrode (reference electrode) attracts positively charged BDNF molecules (isoelectric point: 9.43) at pH 7 to the r-GO/PBASE/APT/BSA modified electrode surface, where they bind to the aptamers. This binding interaction induces changes in the surface potential due to charge accumulation in the recognition layer.[47] For optimal detection, the Debye length of the modified aptaEGFET must be comparable to or exceed the size of the recognition element when interacting with BDNF. If the Debye length does not sufficiently overlap with the size of the recognition element, the charge field from the BDNF molecules will be screened, resulting in a significant decrease in detection sensitivity.[48]

$$\lambda_D = \frac{1}{\sqrt{4\pi I_B \sum_i \rho_i z_i^2}} \quad (2)$$

Here, $I_B$ denotes the Bjerrum length (0.7 nm), while $\rho_i$ and $z_i^2$ represent the ion density and valence, respectively. As indicated by eqn (2), the Debye length $\lambda_D$ diminishes with increasing PBS concentration. Previous studies have shown that $\lambda_D$ significantly impacts target detection. Due to the charge screening effect, BioFETs achieve optimal performance in environments with relatively low ionic strength.

To effectively functionalize the electrode, a 0.75 nm thick PBASE layer was employed as a linker between the aptamers and the r-GO sheet. PBASE binds to the r-GO surface *via* π–π interactions involving its aromatic carbon rings. Additionally, the amine group at the terminal end of the aptamer, which participates in the EDC (1-ethyl-3-(dimethylaminopropyl) carbodiimide)-NHS (*N*-hydroxysuccinimide) coupling reaction with PBASE, measures approximately 0.91 nm. Based on BDNF molecular weight (27 000 g $mol^{-1}$) and average protein density (1.37 g $cm^{-3}$), it is approximately 4 nm in size. When bound to the aptamer and PBASE, the overall BDNF–aptamer–PBASE complex measures about 8.91 nm, which falls within the relevant Debye length of roughly 10 nm. Considering the Debye lengths at various PBS concentrations (0.7 nm in 1× PBS, 2.3 nm in 0.1× PBS, 7.3 nm in 0.01× PBS, 10 nm in 0.005× PBS, and 24 nm in 0.001× PBS), we find that in 0.005× PBS, the 8.91 nm BDNF–aptamer complex remains within the 10 nm Debye screening length of the solution.[49–51]

To assess the efficacy of the modified aptaEGFET for BDNF detection, a systematic experimental investigation was performed. This evaluation involved measuring the responses of the modified aptaEGFET to various BDNF concentrations in a PBS buffer solution. Semiconductor parameter analysis (K2450) was employed for characterizing the modified aptaEGFET. The operational mechanism and sensitivity of the modified aptaEGFET were further elucidated by analysing the $V_{gs}$–$I_{ds}$ (gate voltage *vs.* drain current) electrical characteristics, which provided insight into the performance of the sensing platform. Our hypothesis posits that the positively charged

 

BDNF molecules approach and bind to the surface of the modified aptaEGFET. This interaction induces a change in the surface potential ($\psi$) of the electrode. Notably, this change in surface potential directly affects the threshold voltage ($V_T$) at the interface between the electrolyte and the modified aptaEGFET. Consequently, variations in the BDNF concentration ($C$) lead to corresponding changes in $V_T$, which can be mathematically represented by the following relationship (eqn (3)):[52]

$$V_{T(EGFET)} = V_{T(FET)} - \frac{\psi_M}{q} + E_{REF} + \chi^{Sol} - \psi(C) \quad (3)$$

In this context, the $V_T$ of the MOSFET is denoted as $V_{T(FET)}$, representing the gate threshold voltage for each individual MOSFET. The surface potential of the metal gate is expressed as $\psi_M$, while the potential of the reference electrode is defined by $E_{REF}$. Additionally, the surface dipole potential of the buffer solution is represented by $\chi^{Sol}$. This equation highlights that the sensing mechanism relies on detecting changes in electrical properties, specifically the $V_T$, at the interface between the electrolyte and the modified aptaEGFET. These changes apply to the specific binding of BDNF molecules to the aptamers on the electrode surface. This approach facilitates the quantification of BDNF by measuring the alterations in $V_T$ ($\Delta V_T$).

When a voltage is applied to the extended gate, the $\psi$ changes due to the accumulation of positive charges from BDNF binding, resulting in a leftward shift in the $V_{gs}$–$I_{ds}$ curves of the n-channel MOSFET (Fig. 5b) at a constant $V_{ds}$ = 2 V. As illustrated in Fig. 5b, $V_T$ decreases with rising BDNF concentration, reflecting the enhanced carrier density, leading to a higher current through the channel. Additionally, Fig. 5d shows that the relationship between the drain current ($I_{ds}$) and drain voltage ($V_{ds}$) can be utilized to evaluate the responses of r-GO/PBASE/APT/BSA in the presence of BDNF. $I_{ds}$ in the saturation region can be calculated as follows:[47]

$$I_{ds,max} = \frac{\mu_0 C_{OX}}{2} \times \frac{W}{L} \times (V_{ref} - V_T)^2(1 + \lambda V_{ds}), \quad (4)$$

where electron mobility is depicted by $\mu_0$ in the channel with the width-to-length ratio of $W/L$ and length modulation of $\lambda$. The capacitance of the unit cell is shown as $C_{OX}$, and the voltages applied to the reference and drain electrodes are denoted by $V_{ref}$ and $V_T$, respectively.

As depicted in Fig. 5d, the application of a constant gate voltage ($V_g$ = 3 V) correlates with an increase in $I_{ds,max}$ as the BDNF level increases. This enhancement results from the binding interaction between BDNF and the modified aptaEGFET, leading to an increase in the effective voltage applied to the gate and a subsequent rise in $I_d$.

The modified aptaEGFET was evaluated against various BDNF concentrations to validate its detection effectiveness using BDNF aptamers. Fig. 5e illustrates the resulting $I_{ds}$–$V_{gs}$ characteristics fitted using the Hill–Langmuir model, which represents the affinity binding of a BDNF by an aptamer (eqn (5)):[53,54]

$$\Delta V_T = A\frac{(c/K_d)^n}{1 + (c/K_d)^n} + Z. \quad (5)$$

In this model, the maximum signal resulting from all aptamers binding to BDNF is denoted as $A$, the BDNF concentration is $C$, the effective dissociation constant at which half of the aptamers are occupied by BDNF is $K_a$, the Hill coefficient is $n$, and $Z$ is an offset parameter accounting for $\Delta V_T$ in the absence of BDNF.

The best fit to the data yielded the following values: $A$ = 209.8 mV, $K_d$ = 26.4 nM, $n$ = 0.49, and $Z$ = 9.5 mV. The best-fit value for the offset parameter $Z$ = 9.5 mV aligns with the measured responses of the devices exposed to a pure 0.005× PBS buffer. The best-fit value for $K_d$ = 26.4 nM for soluble BDNF falls within the expected range of 0.025–1000 nM. The best-fit value for $n$ = 0.49 suggests negative cooperativity in the binding of BDNF to the modified aptaEGFET, which may be attributed to protein–aptamer interactions upon binding or increased charge carrier scattering with increased ligand binding. The LOD of 0.4 nM was achieved based on the "3$\sigma$" rule.[55,56] The aforementioned LOD is notably significant, given that the normative serum concentrations of BDNF have been documented to range from 8 to 40 ng mL$^{-1}$. Furthermore, the achieved LOD is comparable to that of graphene-based FET sensors reported for the detection of other biomolecules, underscoring the competitive sensitivity of the proposed sensing platform.[57,58]

Real-time monitoring and specificity checking of aptaEGFET for the detection of BDNF were performed by recording the sensor reference voltage ($V_{ref}$) at a constant $I_{gs}$ = 0.6 μA and a voltage of $V_{ds}$ = 2 V (Fig. 5f). No washing steps or reaction buffer changes were used during the measurements. Initially, the electrodes were placed in a 0.005× PBS buffer solution for approximately 30 minutes to stabilize their potential. BDNF targets were then introduced to the sensing surface of the aptaEGFET-modified electrodes functionalized with aptamer probes. Seven different target concentrations (2.5 pM, 25 pM, 0.5 nM, 2.5 nM, 50 nM, 100 nM, and 1 μM) were added consecutively at 30-minute intervals. Each addition of BDNF concentration resulted in clearly distinguishable drops at $V_{ref}$.

The performance of the aptaEGFET in detecting BDNF was benchmarked to previous studies. Table 1 provides a comparative analysis of various biosensors for BDNF detection, showcasing the advantages of our aptaEGFET. This study exhibits superior sensitivity with a low LOD and a broad linear detection range, utilizing an aptaEGFET. This performance aligns it with advanced FET biosensors and makes it comparable to electrochemical and optical sensors. The aptaEGFET presents a reliable candidate for early neurodegenerative disease diagnosis.

# Experimental

## Materials

PBASE, buffer phosphate saline (PBS), ethanolamine, hydrazine monohydrate (85%), DNA aptamer specific to BDNF (5′-$NH_2$-(T20)-GGATTTGAGCTTATGTGGCATAGGTTGCCTGGGTG GGTGGGGTCGGGGAA-3′) and mutated non-binding aptamer

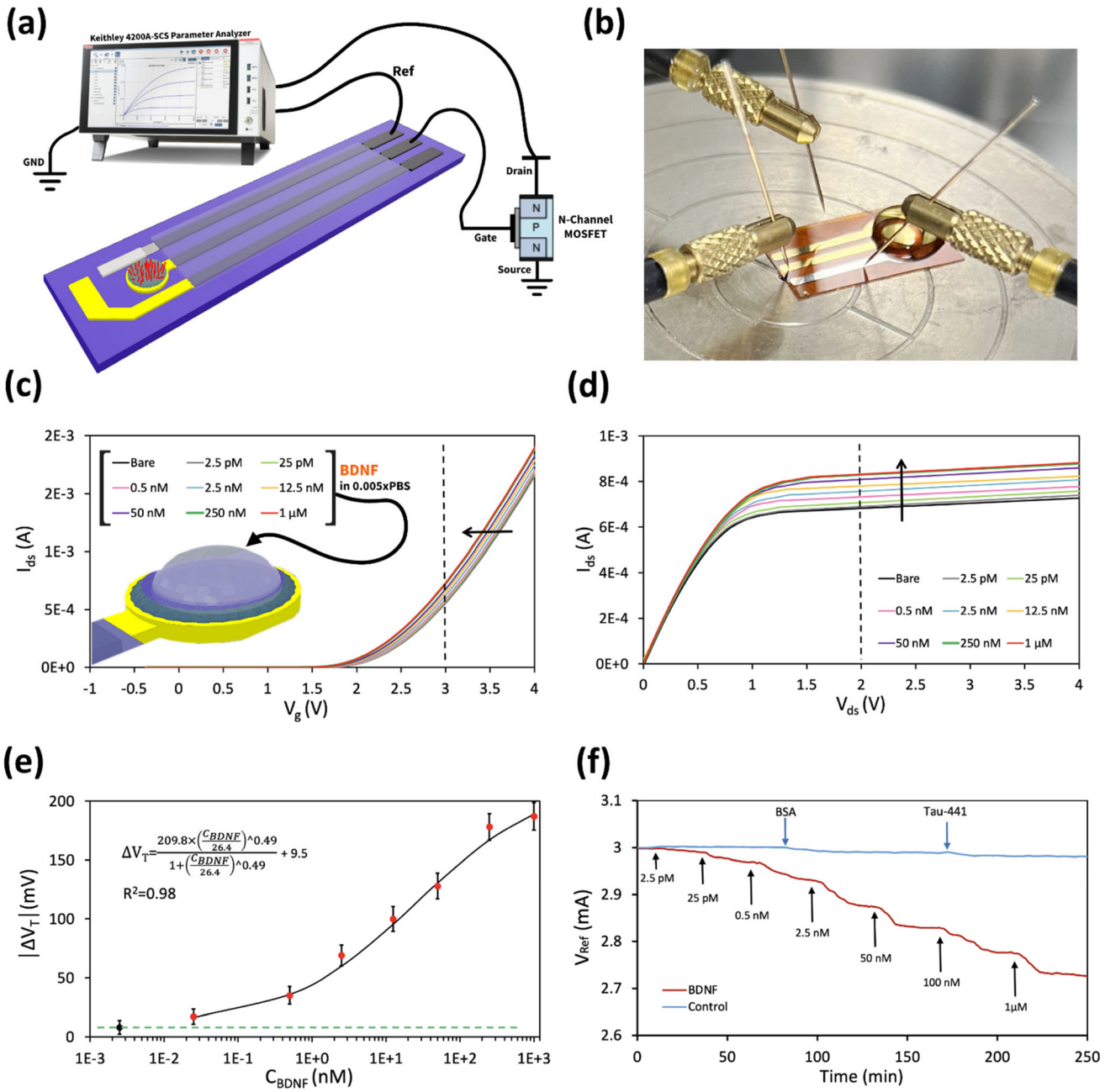


**Fig. 5** (a) The schematic and (b) real image of the aptaEGFET. (c) Gate voltage–drain current – ($I_D$–$V_{gs}$) at $V_D$ = 2 V and (d) drain voltage–drain current ($V_{ds}$–$I_{ds}$) at $V_g$ = 3 V characteristics after applying different concentrations of BDNF to the r-GO/PBASE/APT/BSA modified electrode. (e) The calibration curve and LOD after adding different levels of BDNF. The baseline of the BDNF response, indicated by the green line, is characterized as the mean response augmented by a single standard deviation of three to the r-GO/PBASE/APT/BSA modified electrode of aptaEGFETs when subjected to 0.005× PBS buffer solution in the absence of BDNF. The fitted data to a Hill–Langmuir model for BDNF on the r-GO/PBASE/APT/BSA modified electrode of aptaEGFET are presented. (f) Real-time detection using an aptaEGFET for BDNF detection was investigated. BDNF was added sequentially at different levels. Control samples like BSA and Tau-441 were added at a concentration of 500 nM.

to BDNF (5′-$NH_2$-(T20)-GGATTTGAGCTTATGTGGCATAGGTTG-CCTCCGTGGCTGGCGTCGGGGAA-3′),[65] and $KMnO_4$ (99%), $NaNO_3$ (99%), $H_2O_2$ (30%), $H_2SO_4$ (98%) and graphite (cat. #332461) were purchased from Sigma-Aldrich. Disodium hydrogen phosphate ($Na_2HPO_4$), potassium ferrocyanide ($K_4Fe(CN)_6$), and potassium ferricyanide ($K_3Fe(CN)_6$) were purchased from Merck. The 3.0 µm pore size Whatman membrane filters were purchased from Tisch Scientific. BDNF protein was purchased from Bio-Techne. Double distilled water (DI) was used throughout the work. GDNF, NGF, PSA, and HER2 were purchased from Thermo Fisher Scientific. All chemicals were of analytical grade and used without further

Table 1 Comparison study of different sensors for BDNF detection

| Method | Recognition element | Clinical samples | Limit of detection | Range of detection | Ref. |
|---|---|---|---|---|---|
| Optical | Aptamer | Human serum | 0.2 ng $mL^{-1}$ | 0.41 to 250 ng $mL^{-1}$ | 59 |
| DPV | MIP | — | 9 pg $mL^{-1}$ | 10–40 pg $mL^{-1}$ | 15 |
| EIS | Antibody | Mouse cerebrospinal fluid | — | 10 fg $mL^{-1}$–10 ng $mL^{-1}$ | 46 |
| DPV | Antibody | Human serum | 0.2 ng $mL^{-1}$ | 0.1–2.0 ng $mL^{-1}$ | 60 |
| Colorimetric | Antibody–AuNPs | Artificial tear | 14.12 pg $mL^{-1}$ | 25–300 pg $mL^{-1}$ | 61 |
| EIS | Antibody–AuNPs | Human serum | 1.5 ± 0.012 pg $mL^{-1}$ | 4–600 pg $mL^{-1}$ | 62 |
| CV and DPV | Antibody–MWCNTs | Human serum | 5 pg $mL^{-1}$ | 0.01–100 ng $mL^{-1}$ | 63 |
| CV and DPV | MIP | Human serum | 6 pg $mL^{-1}$ | 0.01–0.06 ng $mL^{-1}$ | 64 |
| EGFET | Aptamer | — | 10.8 ng $mL^{-1}$ (0.4 nM) | 6.7 ng $mL^{-1}$–27 μg $mL^{-1}$ (0.025–1000 nM) | This work |

purification. All solutions were prepared with high-purity nitrogen (99.99% purity) before the experiments. CD4007 (MOSFET) and PI film were purchased from RS Components.

### Fabrication of aptasensors

The glassy carbon electrode (GCE) was cleaned by polishing with 0.05 μm of alumina slurry. 5 μL of GO concentrations up to 0.1 μg $mL^{-1}$ diluted in ultra-pure water (UPW) was drop-cast on the freshly GCE surface. A sealed vessel at 70 degrees Celsius for 3 hours was used to reduce GO to r-GO using hydrazine vapour ($NH_2NH_2{\cdot}xH_2O$, reagent grade, $N_2H_4$: 50–60%). For the immobilization of the DNA aptamers on the electrode surface, 10 mM PBASE in DMF was used to functionalize graphene devices for 120 minutes at room temperature to obtain GC/r-GO/PBASE. Considering the two different moieties of PBASE, it serves two different functions as a heterobifunctional linker.[66,67] PBASE pyrenes stack on the graphene surface by π–π stacking interactions and the succinimide moiety reacts with the amino group at the 5′ end of the probe DNA.[68] To obtain GC/r-GO/PBASE/APT, a total of two microliters of aptamer solution was placed on the GC/r-GO/PBASE electrode surfaces at room temperature for different incubation times and aptamer concentrations in PBS. GC/r-GO/PBASE/APT electrodes were washed with PBS and distilled water for 10 minutes to remove non-attached aptamer molecules. To block unreacted surface sites, this modified electrode was immersed in 1 mg $mL^{-1}$ bovine serum albumin (BSA) solution for 60 minutes. PBS and distilled water were used to thoroughly rinse the electrode after this step. It was named the GC/r-GO/PBASE/APT/BSA electrode. Electrochemical Impedance Spectroscopy (EIS) was used to investigate each step of electrode modification. To detect the BDNF protein, a 2.0 microliter aliquot of the protein was drop-cast on the GC/r-GO/PBASE/APT/BSA electrode for 1 hour. The electrode surface was washed in ultra-pure water and PBS for 10 minutes to remove BDNF that may have remained unabsorbed or weakly absorbed on it. The change in charge transfer resistance ($R_{ct}$) was used as a biosensor response for measuring the concentration of BDNF.

### Apparatus and measurements

An infrared spectrometer equipped with a Jasco 6300 FTIR spectrometer was used to record FTIR spectra of solid-state samples (KBr matrix). The thickness of GO was investigated using an atomic force microscope (AFM) from Park System XE-100E. An Autolab PGSTAT 302N potentiostat/galvanostat (Eco Chemie, Utrecht, Netherlands) was used for all electrochemical measurements. In all electrochemical experiments, a three-electrode system was used with an Ag/AgCl electrode (saturated) in 3 M KCl, a platinum counter electrode, and modified glassy carbon electrodes. EIS was performed in 0.1 M $K_3[Fe(CN)_6]/K_4[Fe(CN)_6]$ at a potential of 0.22 V, with an oscillation potential of 5 mV, at 10 kHz to 0.1 Hz. All electrochemical experiments were conducted at room temperature and pH 7. The modified Randles circuit model was employed to fit the EIS data.

Various concentrations of BDNF ranging from 0.025 to 1000 nM were prepared in 0.005× PBS at pH 7. To examine the EFGET response to different BDNF concentrations, 100 μL of the sample was applied to the surface of a modified electrode for 30 min, followed by rinsing with DI water and gentle drying with $N_2$ gas. This electrode was pre-incubated in a 0.005× PBS solution for 30 minutes to stabilise. Subsequently, the measurement was conducted in a 0.005× PBS solution. The gate voltage ($V_g$) varied from 0 to 5 V, while a constant voltage of 2 V was maintained between the source and drain contacts to ensure that the MOSFET operates in the linear regime. The $I_{ds}$–$V_{gs}$ characteristics of the n-channel MOSFET were documented as the response of the EGFET sensor to various BDNF concentrations. Additionally, $V_g$ was held at a steady 3 V, and the drain voltage ($V_{ds}$) was varied from 0 to 5 V to examine the $I_{ds}$–$V_{ds}$ characteristics of the sensor.

## Conclusions

This study presents a novel electrochemical aptasensor based on reduced-graphene oxide field-effect transistors (r-GO-FETs) for the detection of Brain-Derived Neurotrophic Factor (BDNF). The use of DNA aptamers as recognition elements, combined with the exceptional electrical properties of reduced graphene oxide (r-GO), resulted in a highly sensitive and selective biosensor. By employing Electrochemical Impedance Spectroscopy (EIS) to optimize the sensor, we significantly enhanced sensitivity and achieved a lower limit of detection (LOD), as low as 0.4 nM, and a wide linear response range from 0.025 to 1000 nM. This optimization offers a considerable improvement in sensor performance across a broad dynamic range of BDNF detection.

Additionally, the aptaEGFET exhibited high specificity in complex biological matrices, making it a promising tool for early diagnosis and monitoring of neurodegenerative diseases. The flexible polymer substrate, along with the integration of gold and silver chloride electrodes, further enhanced the stability and performance of the biosensor. This research underscores the potential of aptamer-based biosensors in clinical diagnostics, offering a cost-effective and reliable alternative to conventional methods. Future work will focus on further optimization and clinical validation to establish this technology as a standard diagnostic tool for neurodegenerative disorders.

## Author contributions

Mostafa Salehirozveh: conceptualization, visualization, writing – review & editing, writing – original draft, formal analysis, validation, methodology, investigation, and data curation. Robin Bonné: writing – review & editing and methodology. Peeyush Kumar: investigation and resources. Farbod Abazar: writing – review & editing and software. Parisa Dehghani: writing – review & editing, methodology, and formal analysis. Vellaisamy A. L. Roy: writing – review & editing, resources, project administration, and supervision. Ivan Mijakovic: writing – review & editing, resources, project administration, and supervision.

## Data availability

Additional details on materials, synthesis of GO, substrate preparation, pseudo-reference electrode fabrication, fabrication of flexible aptasensor, electrochemical measurements, electrical setup and analysis, CV analysis of the pseudo-reference electrode, XRD and FTIR characterization studies, fitting EIS parameters of GC electrodes at each functionalization steps, and the long-term monitoring of biosensor performance during 30 days are provided.

## Conflicts of interest

All authors have declared that they have no conflicts of interest.

## Acknowledgements

We gratefully acknowledge funding from the Swedish Research Agency (grant number: 2023-01315 to I. M.) and the Novo Nordisk Foundation (grant number: NNF20CC0035580 to I. M.). The authors extend their gratitude to the James Watt Nanofabrication Centre (JWNC) at the University of Glasgow for their scientific support and to Biosensor Nanotech Ltd, UK, for their technical and industrial contributions.

## References

1 K. F. Azman and R. Zakaria, Recent advances on the role of brain-derived neurotrophic factor (BDNF) in neurodegenerative diseases, *Int. J. Mol. Sci.*, 2022, **23**(12), 6827.
2 G. Tosi, M. A. Vandelli, F. Forni and B. Ruozi, *Nanomedicine and neurodegenerative disorders: so close yet so far*, Taylor & Francis, 2015, pp. 1041–1044.
3 P. Dehghani, V. Jahed and A. Zarrabi, Advances and challenges toward neural regenerative medicine, in *Neural Regenerative Nanomedicine*, 2020, pp. 1–23.
4 M. Salehirozveh, Solid state micro and nanopore sensors for single entity detection, 2023.
5 C.-C. Lin and T.-L. Huang, Brain-derived neurotrophic factor and mental disorders, *Biomed. J.*, 2020, **43**(2), 134–142.
6 P. Dehghani, M. E. Rad, A. Zarepour, P. M. Sivakumar and A. Zarrabi, An insight into the polymeric nanoparticles applications in diabetes diagnosis and treatment, *Mini-Rev. Med. Chem.*, 2023, **23**(2), 192–216.
7 X. Xiong, M. Zeng, X. Peng, C. Feng, C. Li, W. Weng and Y. Li, Serum brain-derived neurotrophic factor (BDNF) as predictors of childhood neuroblastoma relapse, *BMC Cancer*, 2023, **23**(1), 670.
8 H.-y. He, J.-l. Tian, Y.-q. Deng, X. Xiong, Y. Xu, Y.-m. Liao, *et al.*, Association of brain-derived neurotrophic factor levels and depressive symptoms in young adults with acne vulgaris, *BMC Psychiatry*, 2019, **19**, 1–8.
9 K. Saitoh, R. Furihata, Y. Kaneko, M. Suzuki, S. Takahashi and M. Uchiyama, Association of serum BDNF levels and the BDNF Val66Met polymorphism with the sleep pattern in healthy young adults, *PLoS One*, 2018, **13**(6), e0199765.
10 Z. B. Dombi, I. Szendi and P. W. Burnet, Brain derived neurotrophic factor and cognitive dysfunction in the schizophrenia-bipolar spectrum: a systematic review and meta-analysis, *Front. Psychiatry*, 2022, **13**, 827322.
11 M. Balietti, C. Giuli and F. Conti, Peripheral blood brain-derived neurotrophic factor as a biomarker of Alzheimer's disease: are there methodological biases?, *Mol. Neurobiol.*, 2018, **55**, 6661–6672.
12 C. Zhang, X. Wang, Q. Zhu, Y. Mei, Z. Zhang and H. Xu, Decreased serum brain-derived neurotrophic factor in post-stroke depression: a systematic review and meta-analysis, *Front. Psychiatry*, 2022, **13**, 876557.
13 L.-S. Hao, Y. Du, L. Chen, Y.-G. Jiao and Y. Cheng, Brain-derived neurotrophic factor as a biomarker for obsessive-compulsive disorder: A meta-analysis, *J. Psychiatr. Res.*, 2022, **151**, 676–682.
14 Y. Naegelin, H. Dingsdale, K. Säuberli, S. Schädelin, L. Kappos and Y.-A. Barde, Measuring and validating the levels of brain-derived neurotrophic factor in human serum, *eNeuro*, 2018, **5**(2), 0419–17.
15 A. G. Ayankojo, R. Boroznjak, J. Reut, J. Tuvikene, T. Timmusk and V. Syritski, Electrochemical sensor based on molecularly imprinted polymer for rapid quantitative detection of brain-derived neurotrophic factor, *Sens. Actuators, B*, 2023, **397**, 134656.

 

16 G. Presnova, D. Presnov, V. Krupenin, V. Grigorenko, A. Trifonov, I. Andreeva, *et al.*, Biosensor based on a silicon nanowire field-effect transistor functionalized by gold nanoparticles for the highly sensitive determination of prostate specific antigen, *Biosens. Bioelectron.*, 2017, **88**, 283–289.

17 M. Salehirozveh, P. Dehghani and I. Mijakovic, Synthesis, Functionalization, and Biomedical Applications of Iron Oxide Nanoparticles (IONPs), *J. Funct. Biomater.*, 2024, **15**(11), 340.

18 Z.-S. Wu, G. Zhou, L.-C. Yin, W. Ren, F. Li and H.-M. Cheng, Graphene/metal oxide composite electrode materials for energy storage, *Nano Energy*, 2012, **1**(1), 107–131.

19 G. Hu, C. Xu, Z. Sun, S. Wang, H.-M. Cheng, F. Li and W. Ren, 3D Graphene-Foam-Reduced-Graphene-Oxide Hybrid Nested Hierarchical Networks for High-Performance Li-S Batteries, *Adv. Mater.*, 2015, **28**(8), 1603–1609.

20 H. Zhang, H.-M. Cheng and P. Ye, 2D nanomaterials: beyond graphene and transition metal dichalcogenides, *Chem. Soc. Rev.*, 2018, **47**(16), 6009–6012.

21 S. Wang, M. Z. Hossain, K. Shinozuka, N. Shimizu, S. Kitada, T. Suzuki, *et al.*, Graphene field-effect transistor biosensor for detection of biotin with ultrahigh sensitivity and specificity, *Biosens. Bioelectron.*, 2020, **165**, 112363.

22 T. Hayasaka, A. Lin, V. C. Copa, L. P. Lopez Jr, R. A. Loberternos, L. I. M. Ballesteros, *et al.*, An electronic nose using a single graphene FET and machine learning for water, methanol, and ethanol, *Microsyst. Nanoeng.*, 2020, **6**(1), 50.

23 M. Salehirozveh, P. Dehghani, M. Zimmermann, V. A. Roy and H. Heidari, Graphene field effect transistor biosensors based on aptamer for amyloid-β detection, *IEEE Sens. J.*, 2020, **20**(21), 12488–12494.

24 M. Salehirozveh, A. K. Kure Larsen, M. Stojmenovic, F. Thei and M. Dong, In–situ PLL–g–PEG Functionalized Nanopore for Enhancing Protein Characterization, *Chem. – Asian J.*, 2023, **18**(17), e202300515.

25 A. Ambrosetti and P. L. Silvestrelli, Trends in the change in graphene conductivity upon gas adsorption: the relevance of orbital distortion, *J. Phys. Chem. Lett.*, 2020, **11**(7), 2737–2741.

26 P. Sharma, R. Singh, R. Sharma, R. Mukhiya, K. Awasthi and M. Kumar, Palladium-oxide extended gate field effect transistor as pH sensor, *Mater. Lett.:X*, 2021, **12**, 100102.

27 S. K. Alsaee, N. M. Ahmed, E. Mzwd, A. F. Omar, A. Aljameel, N. Afzal, *et al.*, pH sensor based on AuNPs/ITO membrane as extended gate field-effect transistor, *Appl. Phys. B*, 2022, **128**(1), 3.

28 Q. Peng, M. Zhang and G. Shi, High-performance extended-gate field-effect transistor for kinase sensing in Aβ accumulation of Alzheimer's disease, *Anal. Chem.*, 2022, **94**(2), 1491–1497.

29 M.-S. Chae, Y. K. Yoo, J. Kim, T. G. Kim and K. S. Hwang, Graphene-based enzyme-modified field-effect transistor biosensor for monitoring drug effects in Alzheimer's disease treatment, *Sens. Actuators, B*, 2018, **272**, 448–458.

30 J. Zhou, K. Ren, Y. Zheng, J. Su, Y. Zhao, D. Ryan and H. Wu, Fabrication of a microfluidic Ag/AgCl reference electrode and its application for portable and disposable electrochemical microchips, *Electrophoresis*, 2010, **31**(18), 3083–3089.

31 H. Pourzamani, E. Jafari, M. Rozveh, H. Mohammadi, M. Rostami and N. Mengelizadeh, Degradation of ciprofloxacin in aqueous solution by activating the peroxymonosulfate using graphene based on CoFe2O4, *Desalin. Water Treat.*, 2019, **167**, 156–169.

32 Y. Hu, F. Li, X. Bai, D. Li, S. Hua, K. Wang and L. Niu, Label-free electrochemical impedance sensing of DNA hybridization based on functionalized graphene sheets, *Chem. Commun.*, 2011, **47**(6), 1743–1745.

33 D. R. Dreyer, S. Park, C. W. Bielawski and R. S. Ruoff, The chemistry of graphene oxide, *Chem. Soc. Rev.*, 2010, **39**(1), 228–240.

34 T. Al-Gahouari, P. Sayyad, G. Bodkhe, N. Ingle, M. Mahadik, S. Shirsat and M. Shirsat, Controlling reduction degree of graphene oxide-based electrode for improving the sensing performance toward heavy metal ions, *Appl. Phys. A*, 2021, **127**, 1–16.

35 Polymer based nanostructures for innovative bio and immunosensors development. International Conference on Advancements of Medicine and Health Care through Technology; 5th–7th June 2014, ed. L. Fritea, A. Florea, M. Tertiș, A. Cristea, R. Săndulescu and C. Cristea, MEDITECH, Cluj-Napoca, Romania 2014, 2014, Springer.

36 C. S. R. Vusa, S. Berchmans and S. Alwarappan, Facile and green synthesis of graphene, *RSC Adv.*, 2014, **4**(43), 22470–22475.

37 P. Dehghani, V. Karthikeyan, A. Tajabadi, D. S. Assi, A. Catchpole, J. Wadsworth, *et al.*, Rapid Near-Patient Impedimetric Sensing Platform for Prostate Cancer Diagnosis, *ACS Omega*, 2024, **9**(12), 14580–14591.

38 M. A. Ehsan, S. A. Khan and A. Rehman, Screen-printed graphene/carbon electrodes on paper substrates as impedance sensors for detection of coronavirus in nasopharyngeal fluid samples, *Diagnostics*, 2021, **11**(6), 1030.

39 B. Mojsoska, S. Larsen, D. A. Olsen, J. S. Madsen, I. Brandslund and A. FAa, Rapid SARS-CoV-2 detection using electrochemical immunosensor, *Sensors*, 2021, **21**(2), 390.

40 D. S. Sipuka, F. O. Olorundare, S. Makaluza, N. Midzi, T. I. Sebokolodi, O. A. Arotiba and D. Nkosi, Dendrimer—Gold Nanocomposite-Based Electrochemical Aptasensor for the Detection of Dopamine, *ACS Omega*, 2023, **8**(37), 33403–33411.

41 S. Wang, M. Sun, Y. Zhang, H. Ji, J. Gao, S. Song, *et al.*, Ultrasensitive antibiotic perceiving based on aptamer-functionalized ultraclean graphene field-effect transistor biosensor, *Anal. Chem.*, 2022, **94**(42), 14785–14793.

42 G. Saltzgaber, P. M. Wojcik, T. Sharf, M. R. Leyden, J. L. Wardini, C. A. Heist, *et al.*, Scalable graphene field-effect sensors for specific protein detection, *Nanotechnology*, 2013, **24**(35), 355502.

43 J. Varshosaz, E. Ghassami, A. Noorbakhsh, A. Jahanian-Najafabadi and M. Minayian, Implementation of electrochemical impedance spectroscopy to evaluate HER-2 aptamer conjugation to Ecoflex® nanoparticles for docetaxel delivery in breast cancer cells, *J. Appl. Electrochem.*, 2019, **49**, 87–97.

44 D. Tao, B. Shui, Y. Gu, J. Cheng, W. Zhang, N. Jaffrezic-Renault, *et al.*, Development of a label-free electrochemical aptasensor for the detection of Tau381 and its preliminary application in AD and non-AD patients' sera, *Biosensors*, 2019, **9**(3), 84.

45 R. Husna, C. P. Kurup, M. A. Ansari, N. F. Mohd-Naim and M. U. Ahmed, An electrochemical aptasensor based on AuNRs/AuNWs for sensitive detection of apolipoprotein A-1 (ApoA1) from human serum, *RSC Adv.*, 2023, **13**(6), 3890–3898.

46 Y. K. Yoo, J. Lee, J. Kim, G. Kim, S. Kim, J. Kim, *et al.*, Ultrasensitive detection of brain-derived neurotrophic factor (BDNF) in the brain of freely moving mice using an interdigitated microelectrode (IME) biosensor, *Sci. Rep.*, 2016, **6**(1), 33694.

47 M. Dabrowski, P. S. Sharma, Z. Iskierko, K. Noworyta, M. Cieplak, W. Lisowski, *et al.*, Early diagnosis of fungal infections using piezomicrogravimetric and electric chemosensors based on polymers molecularly imprinted with D-arabitol, *Biosens. Bioelectron.*, 2016, **79**, 627–635.

48 C. X. Zhao, J. N. Liu, B. Q. Li, D. Ren, X. Chen, J. Yu and Q. Zhang, Multiscale construction of bifunctional electrocatalysts for long–lifespan rechargeable zinc–air batteries, *Adv. Funct. Mater.*, 2020, **30**(36), 2003619.

49 J. T. Villanueva, Q. Huang, N. O. Fischer, G. Arya and D. J. Sirbuly, Nanofiber-based total internal reflection microscopy for characterizing colloidal systems at the microscale, *J. Phys. Chem. C*, 2018, **122**(38), 22114–22124.

50 L. Diao, Z. Xu, W. Zhang, B. Miao, Y. Hu, Z. Gu and J. Li, Direct Protein Detection in Solutions of High Ionic Strength using Polyethylene Glycol–modified AlGaN/GaN High Electron Mobility Transistors, *Electroanalysis*, 2022, **34**(8), 1372–1380.

51 D. Kwong Hong Tsang, T. J. Lieberthal, C. Watts, I. E. Dunlop, S. Ramadan, A. E. del Rio Hernandez and N. Klein, Chemically functionalised graphene FET biosensor for the label-free sensing of exosomes, *Sci. Rep.*, 2019, **9**(1), 1–10.

52 P. Estrela, A. Stewart, F. Yan and P. Migliorato, Field effect detection of biomolecular interactions, *Electrochim. Acta*, 2005, **50**(25–26), 4995–5000.

53 M. B. Lerner, F. Matsunaga, G. H. Han, S. J. Hong, J. Xi, A. Crook, *et al.*, Scalable production of highly sensitive nanosensors based on graphene functionalized with a designed G protein-coupled receptor, *Nano Lett.*, 2014, **14**(5), 2709–2714.

54 J. N. Weiss, The Hill equation revisited: uses and misuses, *FASEB J.*, 1997, **11**(11), 835–841.

55 J. Homola, Surface plasmon resonance sensors for detection of chemical and biological species, *Chem. Rev.*, 2008, **108**(2), 462–493.

56 J. Li, A. Tyagi, T. Huang, H. Liu, H. Sun, J. You, *et al.*, Aptasensors based on graphene field-effect transistors for arsenite detection, *ACS Appl. Nano Mater.*, 2022, **5**(9), 12848–12854.

57 T. Bungon, C. Haslam, S. Damiati, B. O'Driscoll, T. Whitley, P. Davey, *et al.*, Graphene FET sensors for Alzheimer's disease protein biomarker clusterin detection, *Front. Mol. Biosci.*, 2021, **8**, 651232.

58 C. Haslam, S. Damiati, T. Whitley, P. Davey, E. Ifeachor and S. A. Awan, Label-free sensors based on graphene field-effect transistors for the detection of human chorionic gonadotropin cancer risk biomarker, *Diagnostics*, 2018, **8**(1), 5.

59 S. Gao, Q. Li, S. Zhang, X. Sun, X. Zheng, H. Qian and J. Wu, One-step high-throughput detection of low-abundance biomarker BDNF using a biolayer interferometry-based 3D aptasensor, *Biosens. Bioelectron.*, 2022, **215**, 114566.

60 M. Bockaj, B. Fung, M. Tsoulis, W. Foster and L. Soleymani, Method for electrochemical detection of brain derived neurotrophic factor (BDNF) in plasma, *Anal. Chem.*, 2018, **90**(14), 8561–8566.

61 Y. Wu, Y. Hu, N. Jiang, R. Anantharanjit, A. K. Yetisen and M. F. Cordeiro, Quantitative brain-derived neurotrophic factor lateral flow assay for point-of-care detection of glaucoma, *Lab Chip*, 2022, **22**(18), 3521–3532.

62 M. H. Akhtar, K. K. Hussain, N. Gurudatt, P. Chandra and Y.-B. Shim, Ultrasensitive dual probe immunosensor for the monitoring of nicotine induced-brain derived neurotrophic factor released from cancer cells, *Biosens. Bioelectron.*, 2018, **116**, 108–115.

63 . Label-free electrochemical detection of brain-derived neurotrophic factor based on a novel immune microelectrode array. 2017 IEEE 17th International Conference on Nanotechnology (IEEE-NANO), ed. H. Xu, J. Luo, Y. Wang, Y. Song, L. Wang and X. Cai, 2017, IEEE.

64 A. Kidakova, J. Reut, R. Boroznjak, A. Öpik and V. Syritski, Advanced sensing materials based on molecularly imprinted polymers towards developing point-of-care diagnostics devices, *Proceedings of the Estonian Academy of Sciences*, 2019, **68**(2), 158–167.

65 M. A. Chowdhury, J. M. Collins, D. A. Gell, S. Perry, M. C. Breadmore, S. Shigdar and A. E. King, Isolation and Identification of the High-Affinity DNA Aptamer Target to the Brain-Derived Neurotrophic Factor (BDNF), *ACS Chem. Neurosci.*, 2023, **15**(2), 346–356.

66 I. Prattis, E. Hui, P. Gubeljak, G. S. K. Schierle, A. Lombardo and L. G. Occhipinti, Graphene for biosensing applications in point-of-care testing, *Trends Biotechnol.*, 2021, **39**(10), 1065–1077.

 

67 Interaction of graphene electrolyte gate field-effect transistor for detection of cortisol biomarker, in *AIP Conference Proceedings*, ed. N. N. M. Maidin, R. A. Rahim, N. H. A. Halim, A. S. Z. Abidin, N. A. Ahmad and Z. Lockman, AIP Publishing, 2018.

68 G. Seo, G. Lee, M. J. Kim, S.-H. Baek, M. Choi, K. B. Ku, *et al.*, Rapid detection of COVID-19 causative virus (SARS-CoV-2) in human nasopharyngeal swab specimens using field-effect transistor-based biosensor, *ACS Nano*, 2020, **14**(4), 5135–5142.